Inorganic Chemistry

Article

pubs.acs.org/IC

Cluster Coordination and Photoluminescence Properties of α-Ag_2WO_4 Microcrystals

L. S. Cavalcante,*[,†,‡] M. A. P. Almeida,*[,§] W. Avansi, Jr.,[†] R. L. Tranquilin,[§] E. Longo,[†,§] N. C. Batista,[‡] V. R. Mastelaro,[⊥] and M. Siu Li[⊥]

[†]Universidade Estadual Paulista, P.O. Box 355, CEP, 14801-907 Araraquara, São Paulo, Brazil

[§]Universidade Federal de São Carlos, P.O. Box 676, CEP, 13565-905 São Carlos, São Paulo, Brazil

[‡]Departamento de Química, UESPI-CCN, Rua João Cabral, P.O. Box 2231, 64002-150 Teresina-PI, Brazil

[⊥]IFSC-Universidade de São Paulo, P.O. Box 369, 13560-970 São Carlos, São Paulo, Brazil

ABSTRACT: In this paper, we report our initial research to obtain hexagonal rod-like elongated silver tungstate (α-Ag_2WO_4) microcrystals by different methods [sonochemistry (SC), coprecipitation (CP), and conventional hydrothermal (CH)] and to study their cluster coordination and optical properties. These microcrystals were structurally characterized by X-ray diffraction (XRD), Rietveld refinements, Fourier transform infrared (FT-IR), X-ray absorption near-edge structure (XANES), and extended X-ray absorption fine structure (EXAFS) spectroscopies. The shape and average size of these α-Ag_2WO_4 microcrystals were observed by field-emission scanning electron microscopy (FE-SEM). The optical properties of these microcrystals were investigated by ultraviolet−visible (UV−vis) spectroscopy and photoluminescence (PL) measurements. XRD patterns and Rietveld refinement data confirmed that α-Ag_2WO_4 microcrystals have an orthorhombic structure. FT-IR spectra exhibited four IR-active modes in a range from 250 to 1000 cm^{-1}. XANES spectra at the W L_3-edge showed distorted octahedral [WO_6] clusters in the lattice, while EXAFS analyses confirmed that W atoms are coordinated by six O atoms. FE-SEM images suggest that the α-Ag_2WO_4 microcrystals grow by aggregation and the Ostwald ripening process. PL properties of α-Ag_2WO_4 microcrystals decrease with an increase in the optical band-gap values (3.19−3.23 eV). Finally, we observed that large hexagonal rod-like α-Ag_2WO_4 microcrystals prepared by the SC method exhibited a major PL emission intensity relative to α-Ag_2WO_4 microcrystals prepared by the CP and CH methods.

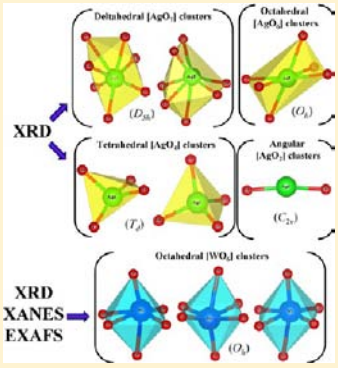

INTRODUCTION

In the past, silver tungstate (α-Ag_2WO_4) ceramics and crystals were initially prepared by different preparation methods such as an oxide mixture or solid-state reaction,[1−4] precipitation/calcination at elevated temperatures,[5] as well as with a crystal growth process named "Czochralski".[6] However, these synthetic methods require high temperatures, longer processing times, and sophisticated equipment with high maintenance costs in addition to the formation of deleterious phases and produce crystals of inhomogeneous sizes and shapes.

In recent years, several synthetic routes were developed and used in the preparation of α-Ag_2WO_4 micro- and nanocrystals. These methods circumvent problems encountered in earlier methods and also facilitate the attainment of these crystals with homogeneous sizes and shapes as well as a single phase. Different synthetic methods are reported in the literature to obtain α-Ag_2WO_4 nanocrystals such as controlled precipitation,[7,8] conventional hydrothermal (CH),[9−11] and microwave hydrothermal.[12] In particular, the CH method was recently used in the preparation of various tungstates with different sizes and shapes.[13−15] Therefore, the conventional/microwave hydrothermal method has received much attention by the scientific community because of its numerous advantages over conventional methods such as the use of an environmentally friendly solvent (water) and low processing temperatures (≤200 °C).[16−18]

According to the literature,[19] the CH method is defined as a processing method for obtaining crystalline materials from the dissolved reagent or soluble precursors in aqueous solution with or without a mineralizer (KOH or NaOH, chemical bases) under temperature and pressure. Generally, the materials obtained by these methods are very fine, crystalline, and are easily dispersed in several solvents.[20] Recently, the CH method was reported in the literature[9,10] for the preparation of α-Ag_2WO_4 nanorods and nanofibers. However, to obtain α-Ag_2WO_4 nanocrystals by this method requires long processing times (12−24 h) due to slow reaction kinetics.[10]

Recently, Wang et al.[21] prepared fine α-Ag_2WO_4 powders with good antimicrobial action by the supersonic-assisted homogeneous precipitation method. In another paper, Hu et al.[22a] obtained irregular particles of α-Ag_2WO_4 powders by microwave-assisted synthesis at different pHs (8 and 10) with photocatalytic activity for the degradation of different organic dyes

Received: May 9, 2012
Published: September 21, 2012

under ultraviolet and visible light. Moreover, Wang and collaborators[22b−d] reported that silver (Ag)-based materials exhibit high photocatalytic properties under visible light for the degradation of methyl orange dye and *Escherichia coli* bacteria destruction.

However, we have found no research literature detailing the coordination number of the atoms for α-Ag_2WO_4 microcrystals and their photoluminescence (PL) properties at room temperature. Therefore, in this paper, we report the synthesis of hexagonal rod-like elongated α-Ag_2WO_4 microcrystals by sonochemistry (SC), coprecipitation (CP), and CH methods. Moreover, these microcrystals were structurally characterized by different techniques to model the cluster coordination and explain their PL properties at room temperature.

EXPERIMENTAL DETAILS

Synthesis of α-Ag_2WO_4 Microcrystals. α-Ag_2WO_4 microcrystals were prepared by SC, CP, and CH methods. The procedure for the typical α-Ag_2WO_4 microcrystal synthesized by the SC method is described as follows: 1×10^{-3} mol of tungstate(VI) sodium dihydrate ($Na_2WO_4{\cdot}2H_2O$; 99.5% purity, Sigma-Aldrich) and 2×10^{-3} mol of silver(I) nitrate ($AgNO_3$; 99.8% purity, Sigma-Aldrich) were dissolved separately in two plastic tubes (Falcon) with 50 mL of deionized water in each tube, and both of the solutions were at pH 6. The first solution with Na^+ and WO_4^{2-} ions was transferred to a 250 mL glass beaker (Boeco, Germany, boro 3.3). Then the second solution at room temperature containing 50 mL of Ag^+ and NO_3^- ions was added to the glass beaker of solution containing the WO_4^{2-} ions; after some seconds, a yellow suspension appeared and a white precipitate rapidly formed. This suspension was ultrasonicated for 1 h in a Branson (model 1510) ultrasonic cleaner with a frequency of 42 kHz. The α-Ag_2WO_4 microcrystal synthesized by the CP method was prepared in the same manner. However, a yellow suspension was maintained at 25 °C, and after 10 min, a white precipitate formed. The α-Ag_2WO_4 microcrystal synthesized by the CH method was prepared in the same manner. However, this suspension and white precipitate were processed in a stainless autoclave at 140 °C for 1 h under a constant 4.5 bar pressure. All of these experimental conditions facilitated stoichiometric chemical reactions ($2Ag^+ + WO_4^{2-}$ ions) that were responsible for the formation of crystalline α-Ag_2WO_4 microcrystals, as shown in eqs 1−3.

After dissolution of the salts at room temperature:

$$Na_2WO_4{\cdot}2H_2O(s) \xrightarrow{H_2O\ (25\ ^\circ C)} 2Na^+(aq) + WO_4^{2-}(aq) + 2H_2O \quad (1)$$

$$2AgNO_3 \xrightarrow{H_2O\ (25\ ^\circ C)} 2Ag^+(aq) + 2NO_3^-(aq) \quad (2)$$

After SC, CP, and CH processing:

$$2Na^+(aq) + WO_4^{2-}(aq) + 2H_2O + 2Ag^+(aq) + 2NO_3^-(aq) \xrightarrow[\approx CH\ (140\ ^\circ C)]{SC\ (70\ ^\circ C)/CP\ (25\ ^\circ C)} \alpha\text{-}Ag_2WO_4(s) + 2Na^+(aq) + 2NO_3^-(aq) + 2H_2O \quad (3)$$

After completion of the SC, CP, and CH processing, the glass beaker and stainless autoclave were naturally cooled to room temperature. The resulting suspensions were washed several times with deionized water and acetone to remove the residual Na^+ ions. Finally, the crystalline α-Ag_2WO_4 microcrystals (light brown in color) were collected and dried with acetone at room temperature for some hours.

Characterization of the α-Ag_2WO_4 Microcrystals. These α-Ag_2WO_4 microcrystals were structurally characterized by X-ray diffraction (XRD) patterns using a D/Max-2000PC diffractometer Rigaku (Japan) with Cu Kα radiation (λ = 1.5406 Å) in the 2θ range from 10° to 70° in the normal routine with a scanning velocity of 2°/min and from 10° to 110° with a scanning velocity of 1°/min in the Rietveld routine. The electronic and local atomic structure around W atoms was checked by using the X-ray absorption spectroscopy (XAS) technique. For XAS measurements, samples were deposited on polymeric membranes. The W L_3-edge XAS spectra of α-Ag_2WO_4 microcrystals were taken at the National Synchrotron Light Laboratory (LNLS) Brazil facility using the D04BXAFS1 beamline. X-ray absorption near-edge structure (XANES) data were collected at the W L_3-edge in transmission mode at room temperature using a Si(111) channel-cut monochromator. XANES spectra were recorded for each sample using an energy step of 1.0 eV before and after the edge and 0.7 and 0.9 eV near the edge region for the W L_3-edge, respectively. Extended X-ray absorption fine structure (EXAFS) spectra were collected between 10100 and 11000 eV using an energy step of 2.0 eV. EXAFS spectra extraction was performed using the Multi-Platform Applications for X-ray absorption (*MAX*) software package,[23] and theoretical spectra were calculated using the *FEFF8.2* code.[24] Fourier transform infrared (FT-IR) spectroscopy was recorded in the range from 250 to 1000 cm^{-1} using KBr pellets as a reference in a Bomem−Michelson spectrophotometer in transmittance mode (model MB-102). The shapes and sizes of these α-Ag_2WO_4 microcrystals were observed with a field-emission scanning electron microscope model Inspect F50 (FEI Company, Hillsboro, OR) operated at 5 kV. UV−vis spectra were taken using a Varian spectrophotometer (model Cary 5G) in a diffuse-reflectance mode. PL measurements were performed through a Monospec 27 monochromator (Thermal Jarrel Ash) coupled to a R446 photomultiplier (Hamamatsu Photonics, Japan). A krypton-ion laser (Coherent Innova 90K; λ = 350 nm) was used as the excitation source; its maximum output power was maintained at 500 mW. The laser beam was passed through an optical chopper, and its maximum power on the sample was maintained at 40 mW. PL measurements were performed at room temperature.

RESULTS AND DISCUSSION

XRD Patterns and Rietveld Refinement Analyses of α-Ag_2WO_4 Crystals. Figure 1 shows XRD patterns for α-Ag_2WO_4 microcrystals prepared by different methods for 1 h in aqueous solutions: SC at 70 °C, CP at 25 °C, and CH at 140 °C.

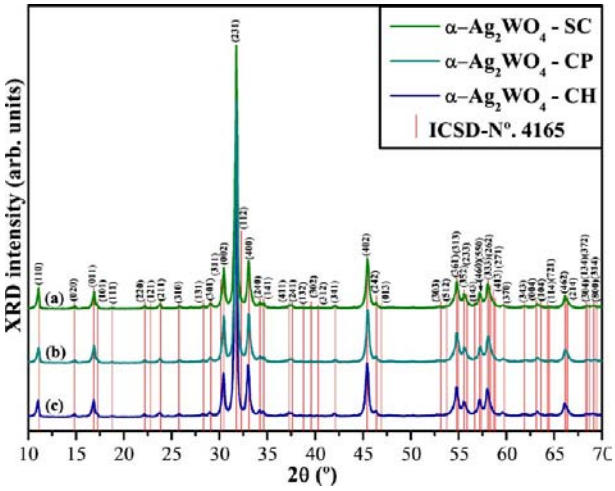

Figure 1. XRD patterns of α-Ag_2WO_4 microcrystals prepared by different methods: (a) SC, (b) CP, and (c) CH. The vertical lines indicate the position and relative intensity of the ICSD card no. 4165 for the α-Ag_2WO_4 phase.

In Figure 1, XRD patterns indicate that all α-Ag_2WO_4 microcrystals have an orthorhombic structure without any deleterious phases with a space group of *Pn2n* and a point-group symmetry of C_{2v}^{10}.[25] These crystals have sharp and well-defined diffraction

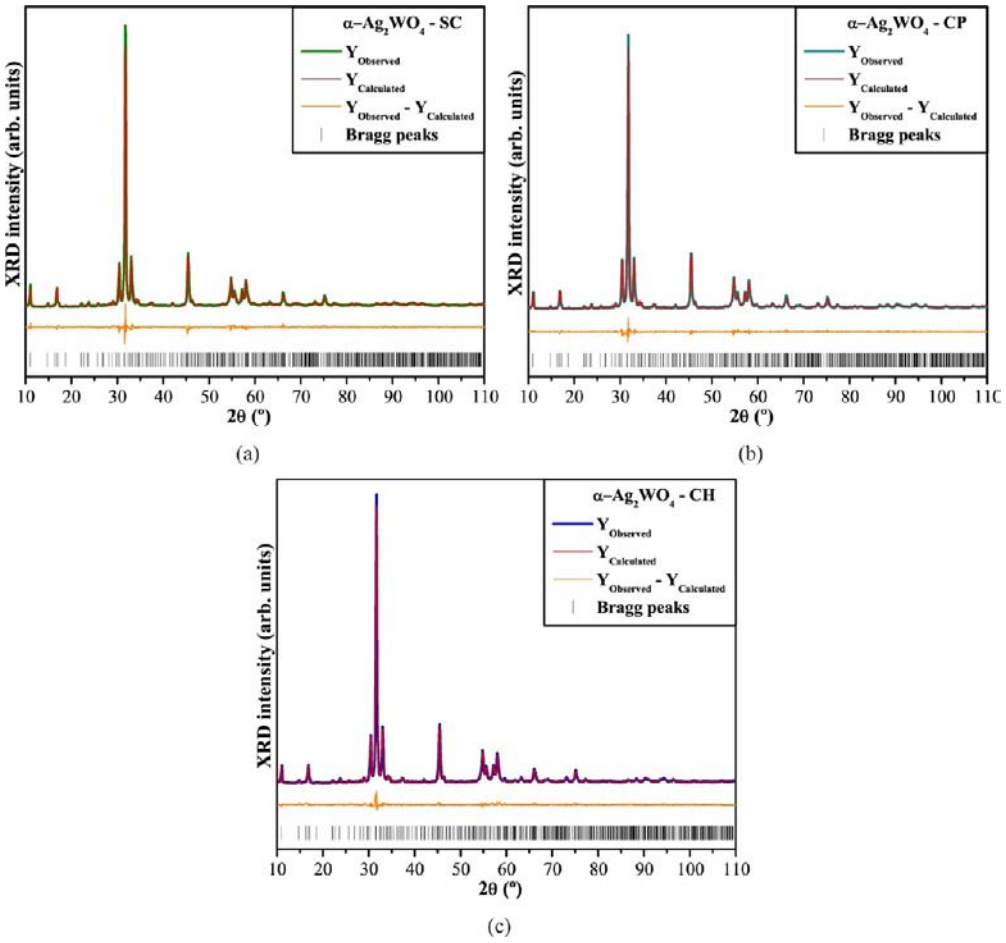

Figure 2. Rietveld refinement plot of α-Ag_2WO_4 microcrystals prepared by different methods: (a) SC, (b) CP, and (c) CH.

peaks, which indicates a reasonable degree of structural order and crystallinity at long range. However, it is difficult to draw any conclusions concerning the existence of Ag nanoparticles in these microcrystals from the XRD measurements.[22d] Moreover, all diffraction peaks are in good agreement with the respective Inorganic Crystal Structure Data (ICSD) base no. 4165[25] and the literature.[26]

Parts a–c of Figure 2 show the Rietveld refinement plot for α-Ag_2WO_4 microcrystals prepared by different methods for 1 h in aqueous solutions: SC at 70 °C, CP at 25 °C, and CH at 140 °C, respectively.

The structural refinement using the Rietveld method[27] was performed to confirm the orthorhombic structure for α-Ag_2WO_4 crystals.[28] According to van den Berg and Juffermans,[29] Ag_2WO_4 microcrystals can exhibit polymorphism; this oxide can have three structure types: α-orthorhombic with a space group of $Pn2n$, β-hexagonal with a space group of $P6_3/m$, and γ-cubic with a space group of $Fd3m$, depending on the pH range (acid or alkaline). In this research, our α-Ag_2WO_4 microcrystals were prepared at pH 6. Therefore, the structural refinement method was employed because it has several advantages over conventional quantitative analysis methods: it employs a whole pattern-fitting algorithm, all lines for each phase are explicitly considered, and even severely overlapped lines are usually not a problem.[30]

The structural refinement was performed using a *Maud* program, version 2.33,[31] which revealed the Rietveld texture and stress analysis.[32] The quality of the structural refinement is generally checked by R values (R_{wnb}, R_b, R_{exp}, R_w, and σ), and these numbers are easy to detect because they are consistent with an orthorhombic structure. However, a difference in the plotting of observed and calculated patterns is the best way to judge the success of the Rietveld refinement.[33] Moreover, other parameters with additional functions were applied to find a structural refinement with better quality and reliability. The optimized parameters were scale factor, background with exponential shift, exponential thermal shift and polynomial coefficients, basic phase, microstructure, crystal structure, size strain (anisotropic and no rules), structure solution model (genetic algorithm SDPD), shift lattice constants, profile half-width parameters (u, v, and w), texture and lattice parameters (a, b, and c), and factor occupancies and atomic site occupancies (Wyckoff). The Rietveld refinement was performed based on the α-Ag_2WO_4 phase with an orthorhombic structure using a better approximation and indexing of the crystallographic information file (CIF) and employing CIF 4165.[25] Therefore, parts a–c of Figure 2 illustrate a good agreement between experimentally observed XRD patterns and theoretically fitted results, which indicates the success of the Rietveld refinement method (see Table 1).

In this table, the fit parameters (R_{wnb}, R_b, R_{exp}, R_w, and σ) suggest that the refinement results are very reliable. There are considerable variations in the atomic positions related to O atoms, while Ag and W atoms practically maintain their fixed positions in the lattice. These results for XRD and Rietveld refinement data indicate different structural distortions and coordination on the $[AgO_y]$ (y = 7, 6, 4, and 2) and $[WO_6]$ clusters at long range,

dx.doi.org/10.1021/ic300948n | *Inorg. Chem.* 2012, 51, 10675–10687

Table 1. Lattice Parameters, Unit Cell Volume, Atomic Coordinates, and Site Occupation Obtained by Rietveld Refinement Data for the α-Ag_2WO_4 Microcrystals Prepared by Different Methods (SC, CP, and CH)

atom[a]	Wyckoff	site	x	y	z
W1	4c	1	0.2541	0	0.5255
W2	2b	..2	0	0.8475	0.5
W3	2b	..2	0	0.1381	0.5
Ag1	4c	1	0.7631	0.1693	0.9748
Ag2	4c	1	0.2434	0.8151	0.0088
Ag3	2a	..2	0	0.9891	0
Ag4	2a	..2	0	0.6661	0
Ag5	2a	..2	0	0.3162	0
Ag6	2a	..2	0	0.5153	0.5
O1	4c	1	0.3542	0.5956	0.2241
O2	4c	1	0.4087	0.3737	0.2252
O3	4c	1	0.4102	0.7381	0.7892
O4	4c	1	0.3821	0.2832	0.7487
O5	4c	1	0.1795	0.4685	0.2160
O6	4c	1	0.4755	0.4632	0.8057
O7	4c	1	0.2508	0.5108	0.8376
O8	4c	1	0.1987	0.3883	0.7642
atom[b]	Wyckoff	site	x	y	z
W1	4c	1	0.2555	0	0.5236
W2	2b	..2	0	0.8475	0.5
W3	2b	..2	0	0.1381	0.5
Ag1	4c	1	0.7536	0.1723	0.9846
Ag2	4c	1	0.2351	0.8171	0.0091
Ag3	2a	..2	0	0.9893	0
Ag4	2a	..2	0	0.6661	0
Ag5	2a	..2	0	0.3164	0
Ag6	2a	..2	0	0.5153	0.5
O1	4c	1	0.3551	0.5956	0.1822
O2	4c	1	0.4067	0.3688	0.1757
O3	4c	1	0.4157	0.7384	0.8092
O4	4c	1	0.3827	0.2782	0.7671
O5	4c	1	0.1812	0.4886	0.2764
O6	4c	1	0.4687	0.4718	0.8276
O7	4c	1	0.2448	0.5886	0.8377
O8	4c	1	0.1924	0.3725	0.8878
atom[c]	Wyckoff	site	x	y	z
W1	4c	1	0.2554	0	0.5251
W2	2b	..2	0	0.8472	0.5
W3	2b	..2	0	0.1392	0.5
Ag1	4c	1	0.7514	0.1706	0.9867
Ag2	4c	1	0.2354	0.8167	0.0095
Ag3	2a	..2	0	0.9884	0
Ag4	2a	..2	0	0.6564	0
Ag5	2a	..2	0	0.3149	0
Ag6	2a	..2	0	0.5101	0.5
O1	4c	1	0.3655	0.6141	0.1987
O2	4c	1	0.3741	0.3772	0.1945
O3	4c	1	0.4252	0.7386	0.7892
O4	4c	1	0.3982	0.2843	0.8012
O5	4c	1	0.1705	0.4879	0.2915
O6	4c	1	0.4125	0.4894	0.8672
O7	4c	1	0.1978	0.6215	0.8791
O8	4c	1	0.1987	0.3881	0.8788

[a] a = 10.878(4) Å, b = 12.009(5) Å, c = 5.895(1) Å; V = 770.09(4) Å^3; Z = 2.R_w = 12.3%; R_{wnb} = 11.42%; R_b = 9.55%; R_{exp} = 6.94%, and σ = 1.88. Ag_2WO_4 microcrystals obtained by the sonochemistry method at 70°C for 1 h (Support Information). [b] a = 10.878(9) Å, b = 12.012(5) Å, c = 5.896(7) Å; V = 770.57(1) Å^3; Z = 2. R_w = 11.2%; R_{wnb} = 10.12%; R_b = 8.87%; R_{exp} = 6.87%, and σ = 1.63. Ag_2WO_4 microcrystals obtained by the coprecipitation method at 25°C (Support Information). [c] a = 10.886(6) Å, b = 12.014(1) Å, c = 5.893(5) Å; V = 770.82(6) Å^3; Z = 2. R_w = 9.13%; R_{wnb} = 7.44%; R_b = 6.7%; R_{exp} = 6.38%, and σ = 1.43. Ag_2WO_4 microcrystals obtained by the hydrothermal conventional method at 140 °C for 1 h (Support Information).

which can be caused by synthetic routes employed in the preparation of α-Ag_2WO_4 microcrystals. Therefore, we have employed the XANES and EXAFS analyses to prove different distortions in octahedral [WO_6] clusters at short range.

XANES and EXAFS Analyses of α-Ag_2WO_4 Crystals. Figure 3 shows XANES spectra of α-Ag_2WO_4 microcrystals prepared by different methods for 1 h in aqueous solutions: (a) SC at 70 °C; (b) CP at 25 °C; (c) CH at 140 °C. Three α-Ag_2WO_4 samples have identical XANES spectra; when compared to the (d) monoclinic WO_3 standard sample, the only difference is observed at the absorption edge white line.

XANES spectra provide qualitative information on the chemical coordination (tetrahedral, square pyramidal, and octahedral) and the spatial arrangement of atoms in environments over the absorber atom (distorted octahedron) and oxidation state.[34] In Figure 3, the peak (×) is attributed to the electronic transition from $2p_{3/2}$ to the vacant 5d orbital.[35] Therefore, the white line reflects the electronic state of vacant d orbitals of the W atom. According to XRD analyses, the α-Ag_2WO_4 structure contains three different W1,2,3 atoms, W1 in sites (1) and W2 and W3 in sites (..2) leading to a set of six different W−O distances varying from 1.733 to 2.22 Å. On the other hand, the m-WO_3 structure also has a distorted local [WO_6] structural unit, with W−O bond lengths varying from 1.75 to 2.20 Å.[36] Thus, the local structure around W atoms in these compounds reveals a significant degree of distortion, and the similarity of after-edge XANES spectra

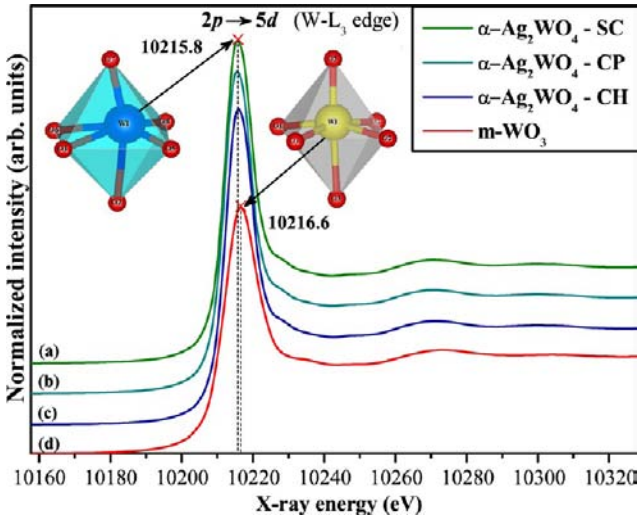

Figure 3. XANES spectra of α-Ag_2WO_4 microcrystals prepared by different methods: (a) SC, (b) CP, and (c) CH and (d) m-WO_3 monoclinic structure (Sigma-Aldrich; 99.9% purity) used as the standard compound.

between α-Ag_2WO_4 and m-WO_3 can be interpreted by the similar degree of distortion around W atoms in these samples (see the inset in Figure 3). According to Yamazoe et al.,[37] the form and profile of the white line region depend on the particular structure

dx.doi.org/10.1021/ic300948n | Inorg. Chem. 2012, 51, 10675−10687

of the compound. Therefore, the difference observed in the absorption-edge white line between the α-Ag_2WO_4 and m-WO_3 samples is probably due to short- and medium-range structural order, which can cause a difference mainly because of the Ag atoms in the α-Ag_2WO_4 lattice.

Parts a and b of Figure 4 illustrate W L_3-edge EXAFS spectra, the respective FT-IR spectra of α-Ag_2WO_4 microcrystals, and the m-WO_3 reference compound.

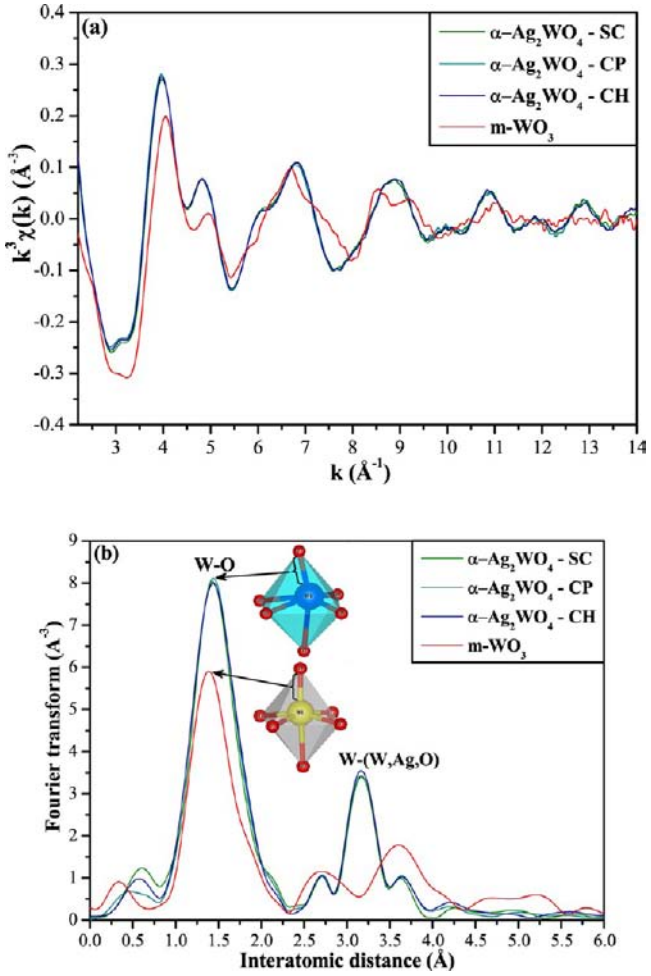

Figure 4. (a) Experimental W L-edge EXAFS signals $k^3\chi(k)$ for the α-Ag_2WO_4 microcrystals prepared by different methods: SC, CP, CH, and m-WO_3 as the reference compound. (b) Experimental signals uncorrected with the Fourier-transformed curve of the α-Ag_2WO_4 microcrystals obtained by different methods and the m-WO_3 standard. The curves are obtained in the 3−14 $Å^{-1}$ k spaces using a hanning window.

EXAFS spectra provide quantitative information on bond distances between atoms (clusters), the coordination number, the calculated distance, and the connecting central atom (clusters) on first- and second-coordination spheres.[34] In good agreement with XANES results, the EXAFS spectra shown in Figure 4(a) and the FT-IR spectra of the α-Ag_2WO_4 microcrystals are practically identical, which confirms that the local structures around the W atoms on the three α-Ag_2WO_4 samples are similar. The lower intensity of the of m-WO_3 compound Fourier-transformed curve can be attributed to a lower coordination number or a higher local disorder around the W atoms. As in all samples, the W atoms are coordinated by six O atoms (see the inset in Figure 4b), and the intensity difference observed in Figure 4b is due to a higher local disorder for the m-WO_3 sample.

To obtain quantitative information from experimental EXAFS spectra, theoretical spectra were calculated using the *FEFF8.2* code[24] according to the long-range-order structure that was previously determined from XRD patterns and Rietveld refinement data. According to these structural models, on the α-Ag_2WO_4 samples, the more intense peak between 1.0 and 2.0 Å in the Fourier transforms corresponds to a single scattering interaction between the first six O atoms and W atoms as the absorber atoms. The peaks located above 2.5 Å correspond to W−(W,Ag,O) interactions, which can be related to single or multiple scattering effects.

The experimental and calculated EXAFS spectra of the α-Ag_2WO_4 sample prepared by SC at 70 °C are shown in Figure 5a,b.

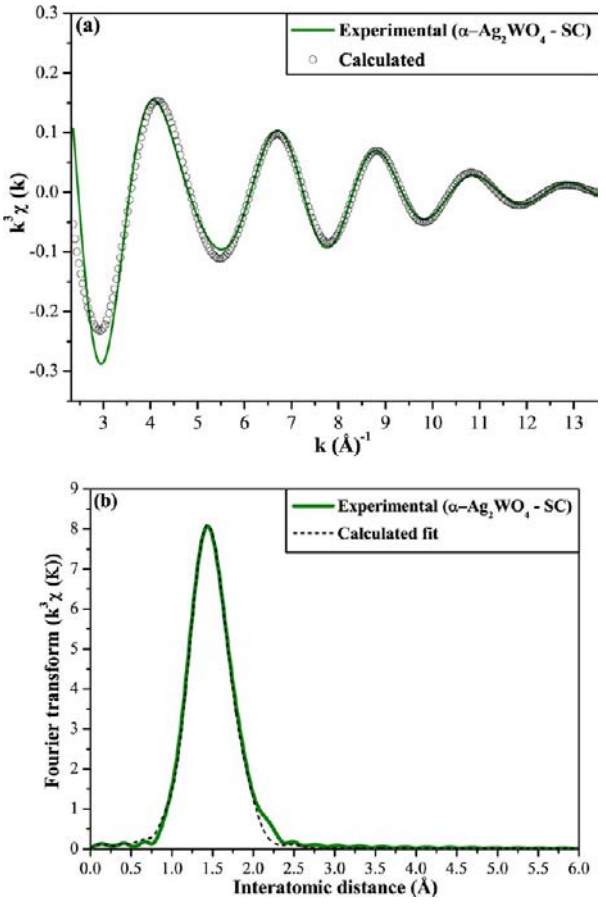

Figure 5. (a) Experimental k^3-weighted EXAFS data (solid line) and back-transformed calculated fit (circles). (b) Fourier-transformed curves obtained from part a: experimental data (solid line) and calculated fit (dashed line).

Quantitative structural data concerning the first-coordination shell around the W atom were modeled by selecting the peak between 1.0 and 2.0 Å of the Fourier-transformed curve (see Figure 5a,b). The fitting of EXAFS spectra corresponding to the first shell was obtained by a Fourier back-transformation of the first peak. In all cases, the number of free parameters was maintained at a lower number than the independent points, which is defined as $N_{ind} = 2\Delta R\Delta K/\pi$, where ΔR is the width of

dx.doi.org/10.1021/ic300948n | *Inorg. Chem.* 2012, 51, 10675−10687

the R space filter windows and ΔK is the actual interval of the fit in the K space.[38] For the m-WO_3 sample fit, the local structural model proposed by Moscovici et al.[36] was used. For the α-Ag_2WO_4 samples, the best-fit procedure was attained when a three W−O coordination shell was used. Parameters varying during the fitting procedure were the number of neighbors (N), the mean bond length (R), the Debye−Waller factor (σ^2), and ΔE_0. The fitting results as well as the reliability determined by a quality factor (QF) are shown in Table 2.

Table 2. Structural Results Obtained from the Fittings of m-WO_3 and α-Ag_2WO_4 Prepared by Different Methods with Filtered EXAFS Spectra Considering Only the First Shell[a]

sample	N	R (Å)	σ^2 (Å^2)	QF
m-WO_3	2.0(2)	1.75(1)	0.0005(2)	2.0
	2.1(3)	1.89(1)		
	2.0(1)	2.08(1)		
	1.1(2)	2.23(1)		
α-Ag_2WO_4-SC	3.5(3)	1.79(1)	0.0030(2)	7.5
	2.0(2)	2.13(1)		
α-Ag_2WO_4-CP	3.8(2)	1.79(1)	0.0033(3)	7.1
	2.2(2)	2.12(1)		
α-Ag_2WO_4-CH	4.1(3)	1.79(1)	0.0040(3)	8.6
	2.5(2)	2.12(1)		

[a] N is the W−O neighbor number, σ^2 is the Debye−Waller factor, R is the W−O distance, and QF is the quality factor.

The fitting results concerning the m-WO_3 sample are similar to the results obtained by Moscovici et al.,[36] which confirms the consistency of our data analysis. As expected, the fitting results of the α-Ag_2WO_4 samples show that the three samples reveal the same local structure, at least at the first W−O coordination shell. The difference observed in the Fourier-transformed intensity between m-WO_3 and α-Ag_2WO_4 microcrystals prepared by the SC method is explained by the fact that (according to the fitting results) in the m-WO_3 sample the first W−O coordination shell is more disordered. Therefore, XANES and EXAFS analyses enabled the identification of two types of W (W1 and W2) clusters. These distortions induce different distance bonds (W−O) in octahedral [WO_6] clusters, and this distortion effect induces the formation of variations in the cluster electronic density.

Unit Cell Representation of α-Ag_2WO_4 Crystals. Figure 6 illustrates a schematic representation for orthorhombic α-Ag_2WO_4 unit cells modeled from Rietveld refinement data.

This unit cell was modeled through the *Visualization for Electronic and Structural Analysis* (*VESTA*) program, version 3.0.9, for Windows[39] using lattice parameters and atomic positions obtained from the Rietveld refinement data shown in Table 1 for α-Ag_2WO_4 microcrystals obtained by the CH method. α-Ag_2WO_4 crystals belong to an orthorhombic structure with a space group of $Pn2n$, a point-group symmetry of C_{2v}^{10}, and two molecular formulas per unit cell (Z = 2).[25] Figure 6 shows that bonds between O−Ag−O and O−W−O atoms were projected out of the unit cell. In these unit cells, all of the W (W1, W2, and W3) atoms are coordinated only to six O atoms, which form distorted [WO_6] clusters with an octahedral configuration, a symmetry group O_h, and octahedron polyhedra (6 vertices, 8 faces, and 12 edges).[40] The [WO_6] clusters are distorted in the α-Ag_2WO_4 crystal lattice. These differences in O−W−O bond angles can lead to different levels of order−disorder and/or distortions in the α-Ag_2WO_4 crystal lattice. In addition, in these unit cells, Ag atoms can exhibit four types of coordination. The Ag1 and Ag2 atoms are coordinated by seven O atoms, forming the deltahedral configuration. Deltahedral [AgO_7] clusters are irregular pentagonal dipyramid polyhedra with symmetry group D_{5h}, which forms 7 vertices, 10 faces, and 15 edges.[41] Ag3 atoms are bonded to six O atoms, which form distorted octahedral [AgO_6] clusters and polyhedra of the type distorted octahedra with symmetry group O_h with 6 vertices, 8 faces, and 12 edges.[40] The Ag4 and Ag5 atoms are coordinated by four O atoms, forming tetrahedral coordination. These tetrahedral [AgO_4] clusters are polyhedra of distorted

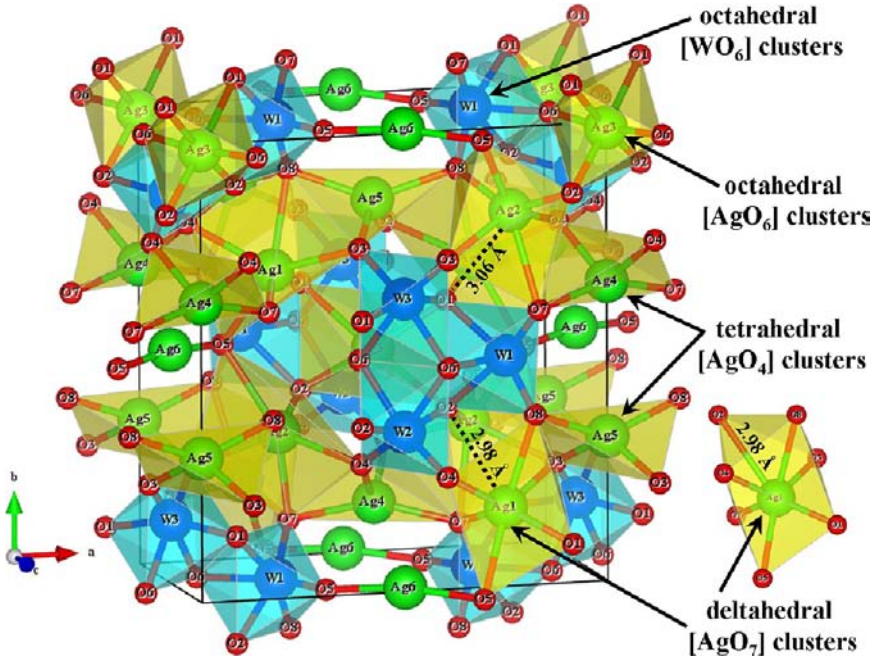

Figure 6. Schematic representation of crystalline unit cells of α-Ag_2WO_4 microcrystals.

dx.doi.org/10.1021/ic300948n | *Inorg. Chem.* 2012, 51, 10675−10687

tetrahedra with symmetry group T_d with 4 vertices, 4 faces, and 6 edges.[42] Moreover, we have observed that Ag4 atoms form distorted tetrahedral [AgO_4] clusters more often than Ag5 atoms, while Ag6 atoms bonded to two O atoms, which form angular [AgO_2] clusters with symmetry group C_{2v} with two vertices.[43] The α-Ag_2WO_4 crystal lattice also contains several distortions on the [AgO_7], [AgO_6], and [AgO_4] clusters through different bond angles within O−Ag−O. XRD, Rietveld refinement, XANES, and EXAFS analyses revealed different levels of distortion on clusters due to the several SC, CP, and CH synthetic methods employed. Moreover, to verify if distorted octahedral [WO_6] cluster vibrations have a specific frequency, which is characteristic of an orthorhombic structure in all α-Ag_2WO_4 microcrystals, FT-IR analyses were performed.

FT-IR Spectroscopic Analyses. Figure 7 shows FT-IR spectra for α-Ag_2WO_4 microcrystals obtained by different methods for 1 h in aqueous solutions: SC at 70 °C, CP at 25 °C, and CH at 140 °C.

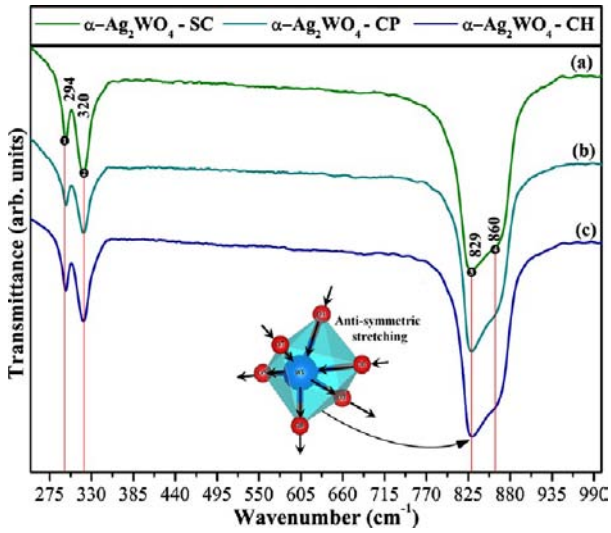

Figure 7. FT-IR spectra of α-Ag_2WO_4 microcrystals prepared by different methods: (a) SC; (b) CP; (c) CH. The vertical lines indicate the position of the IR peaks and IR-active modes.

Figure 7 indicates that four IR-active vibrational modes were experimentally detected. According to the literature,[44] IR spectra provide information on the degree of structural order−disorder in bonds between atoms in ABO_4 materials. Figure 7 verifies two intense absorption bands at 829 and 860 cm^{-1} for all α-Ag_2WO_4 microcrystals. These modes are ascribed to bonds between (←O←W←O←)/(→O→W→O→) of antisymmetric stretching vibrations within distorted [WO_6] clusters (see the inset in Figure 7). The IR-active vibrational internal mode at 320 cm^{-1} is related to symmetric bending vibrations within distorted [WO_6] clusters.[45] Moreover, the IR-active vibrational external mode at 294 cm^{-1} is assigned to the torsional motion of distorted [WO_6] clusters.[46] Peak positions refer to IR-active vibrational modes, which are shown in Table 3, and are compared with other methods as reported in the literature.[7,8,45]

The results reported in Table 3 indicate that all IR-active modes of α-Ag_2WO_4 microcrystals prepared by SC, CP, and CH methods are related to an orthorhombic structure, which is in agreement with the research reported in the literature.[7,8,45] This table verifies that some IR-active-mode relative positions have small shifts, which can be caused by different

Table 3. Comparative Results between the Experimental IR-Active Modes of α-Ag_2WO_4 Microcrystals Obtained in This Work with Those Published in the Literature[a]

M	T (°C)	t (h)	1, vw	2, m	3, s	4, m	ref
SSR	900	24	270	335	800	870	45
SC	70	1	294	320	829	860	×
CP	25	1	294	320	829	860	×
CH	140	1	294	320	829	860	×

[a]M = method; T = temperature; t = time (h); IR modes (cm^{-1}): vw = very weak; m = medium, and s = strong. SSR = solid-state reaction; SC = sonochemistry; CP = coprecipitation; CH = conventional hydrothermal; ref = reference, and × = this work.

factors such as the preparation methods, average crystal size, distortions on O−W−O/O−Ag−O bonds, interaction forces between [WO_6]−[AgO_y] (y = 7, 6, 4, and 2)−[WO_6] clusters, and/or different degrees of structural order−disorder in the lattice at short range.[47] By employing different types of synthetic methods in this research, we obtained field-emission scanning electron microscopy (FE-SEM) images to observe the size, shape, and density of α-Ag_2WO_4 microcrystal superficial defects.

FE-SEM Analyses and Average Size Distribution (Height and Width) of α-Ag_2WO_4 Microcrystals. Parts a−j of Figure 8 show FE-SEM images of α-Ag_2WO_4 microcrystals obtained by different methods for 1 h in aqueous solutions: SC at 70 °C, CP at 25 °C, and CH at 140 °C.

The FE-SEM image in Figure 8a illustrates several rod-like elongated α-Ag_2WO_4 microcrystals with agglomerate nature as well as quasi-monodisperse shapes in a size distribution. These images also indicate that these microcrystals are formed and grow quickly in an aqueous solution after sonication, which promotes a fast precipitation reaction.[48] FE-SEM images in Figure 8b clearly show that these α-Ag_2WO_4 microcrystals are uniform and dense. More details for these α-Ag_2WO_4 microcrystals are illustrated in high magnification in Figure 8c and by the dotted yellow squares in the inset. This figure verifies that α-Ag_2WO_4 microcrystals have a hexagonal rod-like elongated shape. Moreover, some small α-Ag_2WO_4 nanocrystals are visible on large α-Ag_2WO_4 microcrystal surfaces that have not diffused into the interior. Figure 8d shows that α-Ag_2WO_4 microcrystals formed by the CP method at room temperature are well agglomerated with polydisperse shapes in a size distribution. Figure 8e reveals that these α-Ag_2WO_4 microcrystals did not grow because of the low temperature employed by this method. Moreover, Figure 8f confirms several α-Ag_2WO_4 nanocrystals on the surface of these hexagonal rod-like elongated α-Ag_2WO_4 microcrystals. This characteristic can be related to the incomplete diffusion of small crystals to the inside of the larger α-Ag_2WO_4 crystals. Another possible explanation may be attributed to the low thermal energy employed, which promotes a minor rate growth of α-Ag_2WO_4 microcrystals. In addition, one single hexagonal rod-like elongated α-Ag_2WO_4 microcrystal is identifiable (see the inset in Figure 8f). When these precipitated α-Ag_2WO_4 microcrystals are submitted to hydrothermal processing at 140 °C for 1 h, a separation of the majority of the agglomerate α-Ag_2WO_4 microcrystals is observed (see Figure 8g). Moreover, we have also verified that these microcrystals grow by Ostwald-ripening mechanisms and the aggregation of several nanocrystals. According to the literature,[49] hexagonal rod-like elongated α-Ag_2WO_4 microcrystals have grow preferentially in the [001]

dx.doi.org/10.1021/ic300948n | Inorg. Chem. 2012, 51, 10675−10687

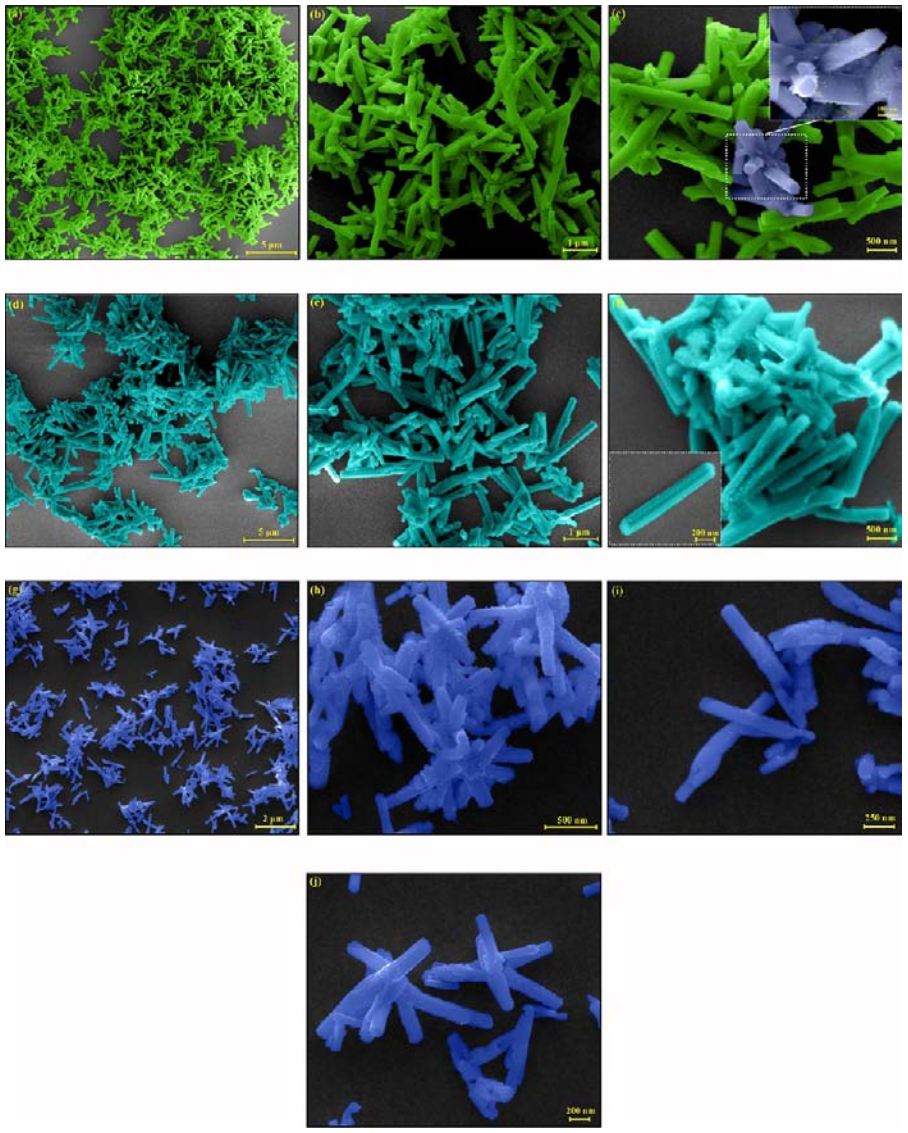

Figure 8. (a) Low-magnification FE-SEM images of α-Ag_2WO_4 microcrystals. (b) Medium-magnification FE-SEM images of α-Ag_2WO_4 microcrystals. (c) High-magnification FE-SEM images (the inset shows the hexagonal rod-like elongated α-Ag_2WO_4 microcrystals obtained from the SC method). (d) Low-magnification FE-SEM images of α-Ag_2WO_4 microcrystals. (e) Medium-magnification FE-SEM images of α-Ag_2WO_4 microcrystals. (f) High-magnification FE-SEM images of hexagonal rod-like elongated α-Ag_2WO_4 microcrystals obtained by the CP method (the inset shows a single hexagonal rod-like elongated α-Ag_2WO_4 microcrystal obtained by the CP method). (g) Low-magnification FE-SEM images of α-Ag_2WO_4 microcrystals. (h) Medium-magnification FE-SEM images of α-Ag_2WO_4 microcrystals. (i and j) High-magnification FE-SEM images of hexagonal rod-like elongated α-Ag_2WO_4 microcrystals obtained by the CH method.

direction. Figure 8h reveals several α-Ag_2WO_4 nanocrystals on the large α-Ag_2WO_4 crystal surface. Figure 8i shows smaller hexagonal rod-like crystals, which possibly were formed after the dissolution of larger crystals under hydrothermal conditions at 4.5 bar of pressure. Moreover, Figure 8i also shows two hexagonal rod-like α-Ag_2WO_4 crystals in aggregation and imperfect growth because the junction between the two crystals does not occur in the same (001) crystallographic plane.[50] Finally, Figure 8j shows some hexagonal rod-like α-Ag_2WO_4 hollow crystals; this characteristic confirms that the dissolution of some hexagonal rod-like elongated α-Ag_2WO_4 microcrystals occurs during hydrothermal processing.

In this research, FE-SEM images were also crucial to evaluating the average crystal size distribution by counting 100 crystals for a good surface contour to ensure the authenticity of the statistical response (see Figure 9a–f).

In all cases, the particle-size counting is described well by the log-normal distribution:

$$y = y_0 + \frac{A}{\sqrt{2\pi}wx} e^{-[\ln(x/x_c)]^2/2w^2} \quad (4)$$

where y_0 is the first value on the y axis, A is the amplitude, w is the width, π is a constant, and x_c is the center value of the distribution curve on the x axis.[51]

Hexagonal rod-like elongated α-Ag_2WO_4 crystals obtained by the SC method exhibited an average size (height) distribution in the range from 0.75 to 3.75 μm (see Figure 9a and inset). In this system, it was estimated that 38% of these microcrystals have an average size of approximately 1.75 μm. Figure 9b shows the average size (width) distribution in the range from 0.2 to 0.32 μm for α-Ag_2WO_4 crystals prepared at 70 °C ultrasonically for 1 h. An estimated 78% of particles exhibited an average

dx.doi.org/10.1021/ic300948n | Inorg. Chem. 2012, 51, 10675–10687

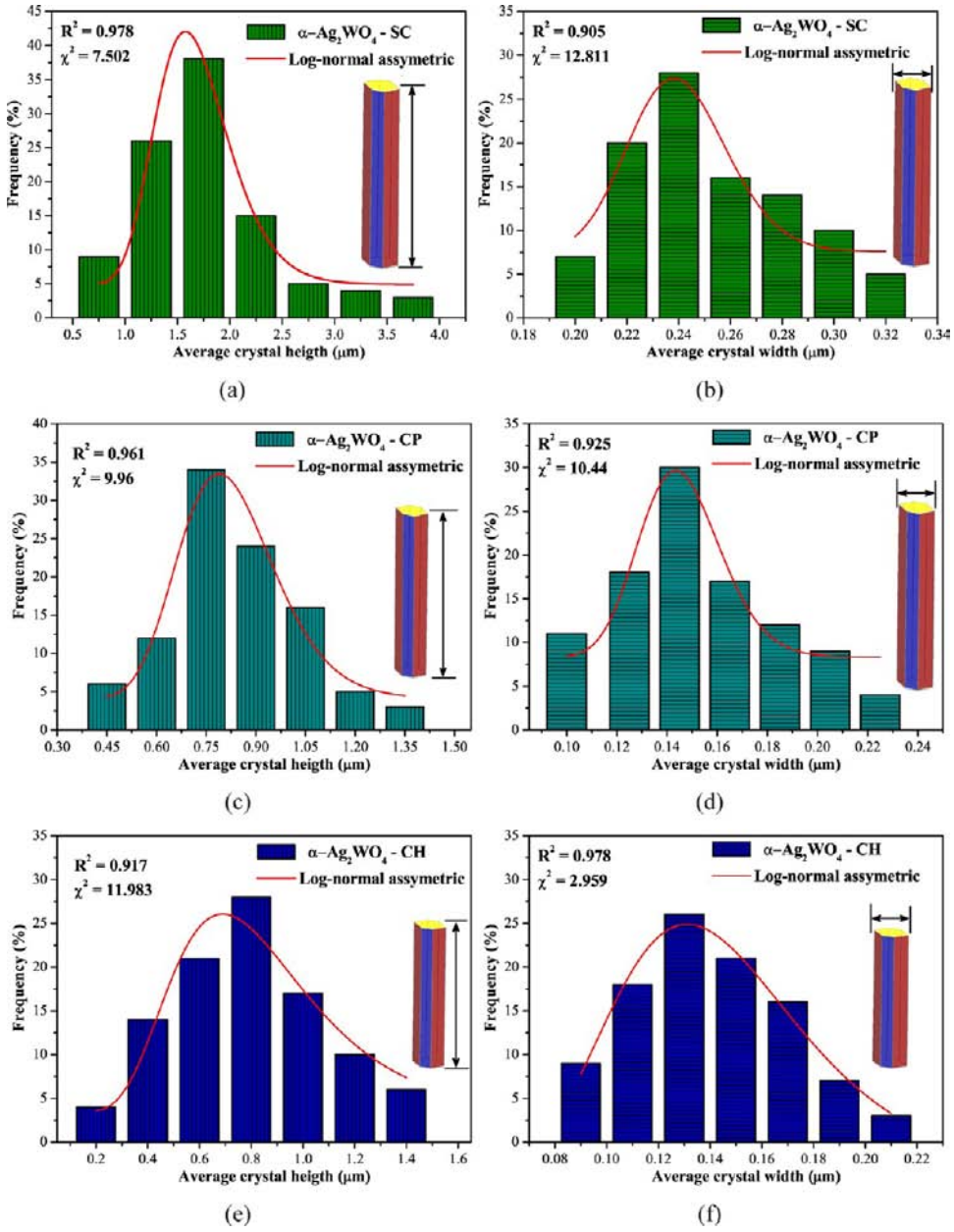

Figure 9. Average height and width distribution of hexagonal rod-like elongated α-Ag_2WO_4 microcrystals obtained by the SC method at 70 °C (a and b), by the CP method at 25 °C (c and d), and by the CH method at 140 °C for 1 h (e and f).

width from 0.22 to 0.28 μm. Figure 9c lists α-Ag_2WO_4 crystals obtained at room temperature by the CP method with an average size (height) distribution from 0.45 to 1.35 μm. Moreover, we have observed that a broadening of the log-normal asymmetric curve occurs, and 37% of these crystals have an average size of 0.75 μm. Additionally, these crystals have an average size (width) distribution from 0.1 to 0.225 μm (see Figure 9d and inset). For hexagonal rod-like elongated α-Ag_2WO_4 crystals obtained by the CH method at 140 °C for 1 h, an increase occurs in the dispersion of the average size (height) distribution, with a range from 0.2 to 1.4 μm. This behavior is illustrated by an increase in the correlation coefficient (R^2) values and the χ^2 distribution, which indicates a major dispersion in the average size (height) distribution prepared under hydrothermal conditions. Finally, these crystals exhibited a reduction in the average size (width) distribution from 0.09 to 0.21 μm (see Figure 9f and inset). A general analysis of the FE-SEM images reveals that the SC method produces α-Ag_2WO_4 crystals double the size in relation to crystals obtained by the CP and CH methods. In addition, we observed the presence of some spherical-like Ag nanoparticles on the hexagonal rod-like elongated α-Ag_2WO_4 microcrystals by means of high-resolution transmission electron microscopy, and electron diffraction confirms its cubic structure. These Ag nanoparticles have an average particle size of 6 nm. However, future observations and explanations for this curious fact will be reported in a future work. To verify possible electronic levels between the valence and conduction bands, UV–vis measurements were taken to characterize optical band-gap values of α-Ag_2WO_4 microcrystals.

UV–Vis Absorption Spectroscopy Analyses of α-Ag_2WO_4 Crystals. The optical band-gap energy (E_{gap}) was calculated by the method proposed by Kubelka and Munk-Aussig.[52] This methodology is based on the transformation of diffuse-reflectance measurements to estimate E_{gap} values with good accuracy within

dx.doi.org/10.1021/ic300948n | Inorg. Chem. 2012, 51, 10675–10687

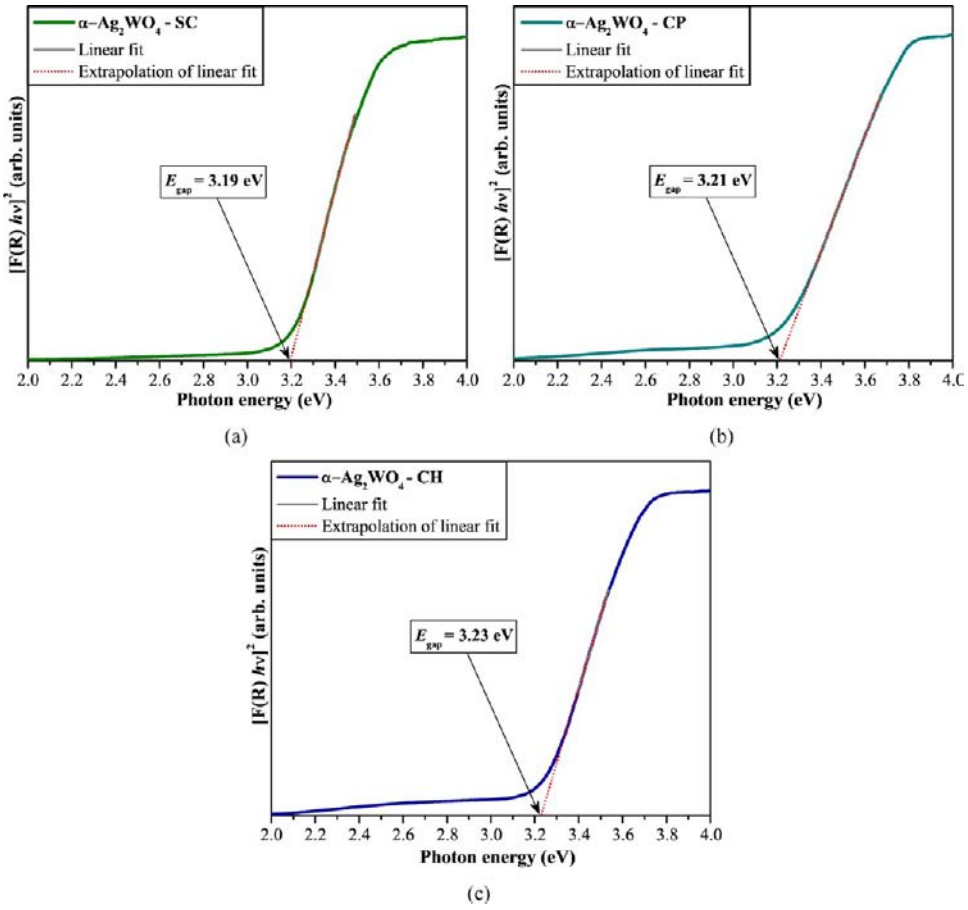

Figure 10. UV–vis spectra of α-Ag_2WO_4 microcrystals prepared by different methods: (a) SC, (b) CP, and (c) CH.

the limits of assumptions when modeled in three dimensions.[53] The Kubelka–Munk equation for any wavelength is described as

$$F(R_\infty) = \frac{(1 - R_\infty)^2}{2R_\infty} = \frac{k}{s} \quad (5)$$

where $F(R_\infty)$ is the Kubelka–Munk function or the absolute reflectance of the sample. In our case, magnesium oxide (MgO) was the standard sample in reflectance measurements. $R_\infty = R_{sample}/R_{MgO}$ (R_∞ is the reflectance when the sample is infinitely thick), k is the molar absorption coefficient, and s is the scattering coefficient. In a parabolic band structure, the optical band gap and absorption coefficient of semiconductor oxides[54] can be calculated by the following equation:

$$\alpha h\nu = C_1(h\nu - E_{gap})^n \quad (6)$$

where α is the linear absorption coefficient of the material, $h\nu$ is the photon energy, C_1 is a proportionality constant, E_{gap} is the optical band gap, and n is a constant associated with different kinds of electronic transitions (n = 0.5 for a direct allowed and n = 2 for an indirect allowed). According to Kim et al.,[55] silver tungstate ($Ag_2W_2O_7$) exhibited an optical absorption spectrum governed by direct electronic transitions between the valence and conduction bands, while silver molybdate ($Ag_2Mo_2O_7$) showed indirect electronic transitions. Therefore, we ascertained that our hexagonal rod-like elongated α-Ag_2WO_4 microcrystals have a direct E_{gap}.[56] On the basis of this information, E_{gap} values of α-Ag_2WO_4 microcrystals were calculated using n = 0.5 in eq 6. Finally, using the remission function described in eq 5 and with the term $k = 2\alpha$ and C_2 as a proportionality constant, we obtained the modified Kubelka–Munk equation, as indicated in eq 7.

$$[F(R_\infty)h\nu]^2 = C_2(h\nu - E_{gap}) \quad (7)$$

Therefore, when the $F(R_\infty)$ value was found from eq 7 and a graph of $[F(R_\infty)h\nu]^2$ against $h\nu$ was plotted, the E_{gap} of α-Ag_2WO_4 microcrystals was determined.

Parts a–c of Figure 10 illustrate UV–vis spectra of α-Ag_2WO_4 microcrystals obtained by different methods for 1 h in aqueous solutions: SC at 70 °C, CP at 25 °C, and CH at 140 °C.

Parts a–c of Figure 10 reveal that the optical band gap for all α-Ag_2WO_4 microcrystals are characterized by well-defined direct electronic transitions, which is the typical nature of crystalline semiconductor materials.[57] The exponential optical absorption edge and the optical band-gap energy are controlled by the degree of structural disorder in the lattice. The increase in the E_{gap} values can be attributed to the reduction of defects in local lattice distortions and localized electronic levels within the forbidden band gap.[58] Moreover, we believe that these differences in the E_{gap} values are mainly attributable to different levels of distortions on both $[AgO_y]$ (y = 7, 6, 4, and 2) and $[WO_6]$ clusters at short and medium range. Also, there is a slight increase in the E_{gap} value for α-Ag_2WO_4 microcrystals obtained by the CH method at 140 °C for 1 h, which can possibly be related to a slight reduction in the structural disorder, distortion level of the clusters, and electronic intermediate levels between the valence and conduction bands. Therefore, the techniques employed above indicate that three types of α-Ag_2WO_4 crystals are formed by different $[AgO_y]$ (y = 7, 6, 4, and 2) and

dx.doi.org/10.1021/ic300948n | Inorg. Chem. 2012, 51, 10675–10687

$[WO_6]$ clusters. However, this fact can only be proven with a PL technique to the molecular level at medium range that differentiates the defect density among α-Ag_2WO_4 microcrystal clusters prepared by SC, CP, and CH methods. The PL properties are an important tool that provides fundamental information about structural defects and/or the degree of cluster distortion in the lattice.

PL Properties of α-Ag_2WO_4 Microcrystals. Figure 11 illustrates PL spectra at room temperature for α-Ag_2WO_4

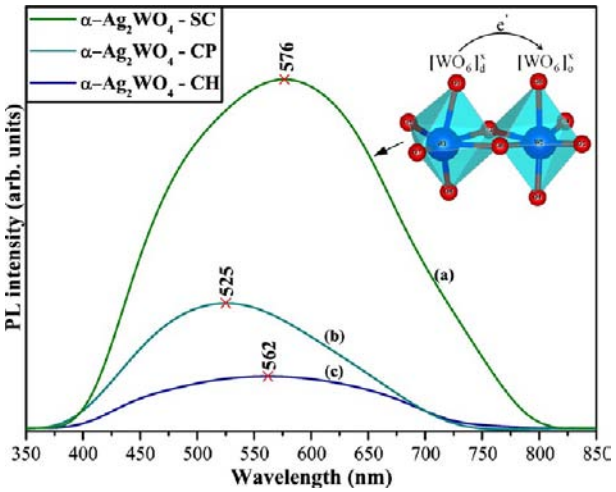

Figure 11. PL spectra of hexagonal rod-like elongated α-Ag_2WO_4 microcrystals prepared by different methods: (a) SC; (b) CP; (c) CH. The inset shows the possible mechanism of electronic transfer between the distorted octahedral $[WO_6]^x_d$ and undistorted octahedral $[WO_6]^x_o$ clusters.

microcrystals obtained by different methods for 1 h in aqueous solutions: SC at 70 °C, CP at 25 °C, and CH at 140 °C.

PL spectral profiles have a typical behavior for multiphonon or multilevel processes, i.e., a solid system where the relaxation occurs by several pathways, which involve the participation of numerous energy states within the band gap.[59] In general, PL emission spectra of silver tungstates (Ag_2WO_4 and $Ag_2W_2O_7$) are frequently decomposed into blue- and green-light components.[60,61] In this research, the PL behavior is explained by photogenerated electron–hole pair (excitons) processes and in terms of the electronic transition between the valence band (2p levels of O atoms and 4d levels of Ag atoms) and the conduction band (5d levels of W atoms). In this report, we confirm that structural defects in the α-Ag_2WO_4 microcrystal lattice are responsible for the appearance of intermediate levels between the valence and conduction bands, which are favorable to intense PL emission properties at room temperature. Figure 11a shows that α-Ag_2WO_4 microcrystals obtained by the SC method exhibit a maximum PL emission at 575 nm in the yellow region of visible spectra. As was noted previously, these microcrystals have a minor E_{gap} value (3.19 eV) not found in other crystals. Therefore, these crystals have favorable conditions to promote the process of charge transfer from distorted $[WO_6]^x_d$ clusters to undistorted $[WO_6]^x_o$ clusters. This electronic transition between clusters probably occurs when α-Ag_2WO_4 microcrystals with distorted clusters are able to absorb photons ($h\nu$) with a particular wavelength (λ) before the excitation process. After the excitation process, the recombination of the electron–hole pair in α-Ag_2WO_4 microcrystals results in the emission of photons ($h\nu'$; lower emission energy than the emission energy found in absorbed photons). Parts b and c of Figure 11 show a reduction in the PL emission intensity for α-Ag_2WO_4 microcrystals prepared by the CP method with a maximum PL emission at 525 nm, which is the green region in visible spectra, and α-Ag_2WO_4 microcrystals prepared by the CH method with a maximum PL emission at 562 nm, which is also in the green region in visible spectra. This behavior can be related to an increase in the E_{gap} values [3.21 eV (CP) and 3.23 eV (CH)] and a reduction in the electronic intermediate levels between conduction and valence bands. Therefore, a considerable reduction in the optical band-gap values is probably linked to $[AgO_y]/[WO_6]$ cluster distortions that are favorable to the formation of intermediate levels between the valence and conduction bands, which indicates an individual E_{gap} value for each α-Ag_2WO_4 microcrystal. Consequently, we assign it to an intrinsic mechanism for PL emission, which is derived mainly from octahedral $[WO_6]$ cluster distortions (see the inset in Figure 11). From a theoretical point of view, these distortions and processes of symmetry breaking between clusters are related to order–disorder effects in the crystal structures, which are necessary conditions for the PL properties in crystals. In addition, these structural defects cause a polarization between clusters that facilitates the population of electronic excited states. Once these excited states are populated, they may return to lower energy and fundamental states via radiative and/or nonradiative relaxations.

In this typical semiconductor, the α-Ag_2WO_4 microcrystal lattice can have different types of characteristics in its electronic structure such as the intercluster (intermediary range) and intracluster (local range) interaction, which can be due to three different sources: orientation, induction, and dispersion interactions.[56] The orientation interaction is associated with the correlation between the rotational motion of permanent moments in different $[WO_6]$–$[WO_6]$, $[AgO_7]$–$[AgO_6]$, $[AgO_7]$–$[AgO_4]$, $[AgO_7]$–$[AgO_2]$, $[WO_6]$–$[AgO_7]$, $[WO_6]$–$[AgO_6]$, $[WO_6]$–$[AgO_4]$, or $[WO_6]$–$[AgO_2]$ complex clusters (medium range). The induction interaction occurs via polarization processes of $[AgO_y]$ (y = 7, 6, 4, and 2) or $[WO_6]$ clusters by the permanent moment of other neighboring $[WO_6]$ or $[AgO_y]$ (y = 7, 6, 4, and 2) clusters (short range). The dispersion interaction arises from the correlation between electrons situated in the neighborhood of $[WO_6]$ or $[AgO_y]$ (y = 7, 6, 4, and 2) clusters (long range).[56]

The cluster-to-cluster charge transfer (CCCT) in a α-Ag_2WO_4 crystal containing more than one kind of cluster is characterized by excitations involving electronic transitions from one cluster to another cluster. In this research, we have attributed and explained these equations with the first-principles quantum-mechanical calculations based on the density functional theory in the B3LYP level (preliminary calculations). Therefore, the main difference in PL spectra of α-Ag_2WO_4 microcrystals can be attributed to the ratio between ordered $[WO_6]_o/[AgO_y]_o$ (y = 7, 6, 4, and 2) clusters and disorder/distorted $[WO_6]_d/[AgO_y]_d$ (y = 7, 6, 4, and 2) clusters. The order–disorder effect or structural distortions remaining in the lattice promote a constant electronic charge transfer between the ordered (o) and disordered/distorted (d) clusters, which is possible according to eqs 8–14:

$$[WO_6]^x_o + [WO_6]^x_d \rightarrow [WO_6]_o' + [WO_6]^{\bullet}_d \quad (8)$$

$$[AgO_7]^x_o + [AgO_7]^x_d \rightarrow [AgO_7]_o' + [AgO_7]^{\bullet}_d \quad (9)$$

dx.doi.org/10.1021/ic300948n | Inorg. Chem. 2012, 51, 10675–10687

$$[AgO_6]_o^x + [AgO_6]_d^x \rightarrow [AgO_6]_o' + [AgO_6]_d^\bullet \quad (10)$$

$$[AgO_4]_o^x + [AgO_4]_d^x \rightarrow [AgO_4]_o' + [AgO_4]_d^\bullet \quad (11)$$

$$[AgO_2]_o^x + [AgO_2]_d^x \rightarrow [AgO_2]_o' + [AgO_2]_d^\bullet \quad (12)$$

$$[WO_6]_o^x + [AgO_y]_d^x \ (y = 7,\ 6,\ 4,\ \text{and}\ 2) \rightarrow [WO_6]_o' + [AgO_y]_d^\bullet \ (y = 7,\ 6,\ 4,\ \text{and}\ 2) \quad (13)$$

$$[AgO_y]_o' \ (y = 7,\ 6,\ 4,\ \text{and}\ 2) + [WO_6]_d^x \rightarrow [AgO_y]_o^x \ (y = 7,\ 6,\ 4,\ \text{and}\ 2) + [WO_6]_d^\bullet \quad (14)$$

Thus, these $[WO_6]_d^\bullet$–$[WO_6]_o'$, $[AgO_7]_d^\bullet$–$[AgO_7]_o'$, $[AgO_6]_d^\bullet$–$[AgO_6]_o'$, $[AgO_4]_d^\bullet$–$[AgO_4]_o'$, $[AgO_2]_d^\bullet$–$[AgO_2]_o'$, $[AgO_y]_d^\bullet$ (y = 7, 6, 4, and 2)–$[WO_6]_o'$, and $[WO_6]_d^\bullet$–$[AgO_y]_o'$ (y = 7, 6, 4, and 2) clusters in pairs have extrinsic defects, which are linked to order–disorder effects in the electronic structure, surfaces, and interfaces commonly verified in tungstate-type materials synthesized by chemical methods.[62,63] These defects create additional energy states above the valence band and below the conduction band, which decrease the band gap.

Finally, structural and electronic reconstructions of all possible combinations between the clusters belonging to a specific crystal are essential to understanding the CCCT process and its influences on the PL phenomenon. In this case, the band-gap increase (as shown by UV–vis measurements) promotes a reduction in the intermediate levels between the valence and conduction bands and, consequently, a decrease in the PL emission intensities. However, the true factor acting on the PL behavior of α-Ag_2WO_4 microcrystals is still not completely clear. Therefore, a detailed study on the electronic structure of α-Ag_2WO_4 crystals with ab initio calculations to verify the importance of $[WO_6]$ clusters in PL emission and the influence of different $[AgO_y]$ (y = 7, 6, 4, and 2) clusters in the lattice will be the subject of further research.

CONCLUSIONS

In summary, we report the easy obtention of hexagonal rod-like elongated α-Ag_2WO_4 microcrystals by different SC, CP, and CH synthetic methods. XRD patterns and Rietveld refinement data indicate that these crystals are monophasic with an orthorhombic structure. Structural refinement data were employed to model $[AgO_y]$ (y = 7, 6, 4, and 2) and $[WO_6]$ clusters. FT-IR spectra exhibited four modes, which indicate that all crystals have high distortions on (O–W–O)/(O–Ag–O) bonds and interaction forces between $[WO_6]$ and $[AgO_y]$ (y = 7, 6, 4, and 2) clusters. According to XANES and EXAFS spectral analyses, the local structure around the W atoms is disordered and composed of three different coordination shells. Moreover, the local coordination structures for the W atoms are similar in all microcrystals. FE-SEM images showed that microcrystals grow by the Ostwald-ripening mechanism and aggregation of small nanocrystals with further growth to hexagonal rodlike elongated α-Ag_2WO_4 microcrystals. UV–vis spectra indicated that α-Ag_2WO_4 microcrystals obtained by the CH method at 140 °C for 1 h have minor intermediate energy levels between the valence and conduction bands. A maximum PL emission at room temperature was observed for α-Ag_2WO_4 microcrystals prepared by the SC method. The PL behavior was explained in terms of a minor dispersion in the average size (height/width) distribution and the presence of intermediate energy levels, which promote favorable electronic transitions between the $[WO_6]_o$ and $[WO_6]_d$ clusters with order–disorder structural at medium range.

AUTHOR INFORMATION

Corresponding Author

*E-mail: laeciosc@bol.com.br (L.S.C.), almeida.pinheiroa@gmail.com (M.A.P.A.).

Notes

The authors declare no competing financial interest.

ACKNOWLEDGMENTS

The authors are thankful for financial support from the Brazilian research financing institutions CNPq-Postdoctorate (159710/2011-1), FAPESP (No. 2009/53189-8), FAPEPI-GERATEC (No. 01.08.0506.00), and CAPES.

REFERENCES

(1) Beg, M. A.; Jain, A. *Polyhedron* **1992**, *11*, 2775.
(2) Michal, R.; Saeger, K. E. *IEEE Trans. Compon., Hybrids, Manufact. Technol.* **1989**, *12*, 71.
(3) Beg, M. A.; Jain, A.; Ghouse, K. M. *J. Solid State Chem.* **1988**, *75*, 1.
(4) Jain, A.; Beg, M. A. *Polyhedron* **1995**, *14*, 2293.
(5) Sienko, M.; Mazumder, B. R. *J. Am. Chem. Soc.* **1960**, *82*, 3505.
(6) Turkovic, A.; Fox, D. L.; Scott, J. F.; Geller, S.; Ruse, G. F. *Mater. Res. Bull.* **1977**, *12*, 189.
(7) George, T.; Joseph, S.; Mathew, S. *Pramana J. Phys.* **2005**, *60*, 793.
(8) Mckechnie, J. S.; Tuner, L. D. S.; Vincent, C. A.; Bonino, F.; Lazzari, M.; Rivolta, B. *J. Inorg. Nucl. Chem.* **1979**, *41*, 177.
(9) Yu, S. H.; Liu, B.; Mo, M. S.; Huang, J. H.; Liu, X. M.; Qian, Y. T. *Adv. Funct. Mater.* **2003**, *13*, 639.
(10) Cui, X.; Yu, S. H.; Li, L.; Biao, L.; Li, H.; Mo, M.; Liu, X. M. *Chem.—Eur. J.* **2004**, *10*, 218.
(11) Wang, P.; Huang, B.; Zhang, X.; Qin, X.; Dai, Y.; Jin, H.; Wei, J.; Whangbo, M. H. *Chem.—Eur. J.* **2008**, *14*, 10543.
(12) Hu, B.; Wu, L. H.; Liu, S. J.; Yao, H. B.; Shi, H. Y.; Li, G. P.; Yu, S. H. *Chem. Commun.* **2010**, *46*, 2277.
(13) Tian, G.; Sun, S. *Cryst. Res. Technol.* **2011**, *46*, 389.
(14) Tawde, D.; Srinivas, M.; Murthy, K. V. R. *Phys. Status Solidi A* **2011**, *208*, 803.
(15) Tian, Y.; Hua, G.; Xu, W.; Li, N.; Fang, M.; Zhang, L. *J. Alloys Compd.* **2011**, *509*, 724.
(16) Siqueira, K. P. F.; Moreira, R. L.; Valadares, M.; Dias, A. *J. Mater. Sci.* **2010**, *45*, 6083.
(17) Guoqiang, T.; Yuqin, Z.; Ao, X.; Yan, W.; Wei, Z. *J. Chin. Ceram. Soc.* **2011**, *39*, 43.
(18) Lei, F.; Yan, B.; Chen, H. H.; Zhang, Q.; Zhao, J. T. *Cryst. Growth Des.* **2009**, *9*, 3730.
(19) Sōmiya, S.; Roy, R. *Bull. Mater. Sci.* **2000**, *23*, 453.
(20) Abothu, I. R.; Liu, S. F.; Komarneni, S.; Li, Q. H. *Mater. Res. Bull.* **1999**, *34*, 1411.
(21) Wang, Q.; Gou, X.; Wu, W.; Liu, S. *Adv. Mater. Res.* **2011**, *284*, 1321.
(22) (a) Hu, B.; Wu, L. H.; Zhao, Z.; Zhang, M.; Chen, S. F.; Liu, S. F.; Shi, H. Y.; Ding, Z. J.; Yu, S. H. *Nano Res.* **2010**, *3*, 395. (b) Wang, P.; Huang, B.; Qin, X.; Zhang, X.; Dai, Y.; Wei, J.; Whangbo, M. H. *Angew. Chem., Int. Ed.* **2008**, *47*, 7931. (c) Wang, P.; Huang, B.; Lou, Z.; Zhang, X.; Qin, X.; Dai, Y.; Zheng, Z.; Wang, X. *Chem.—Eur. J.* **2010**, *16*, 538. (d) Wang, P.; Huang, B.; Qin, X.; Zhang, X.; Dai, Y.; Whangbo, M. H. *Inorg. Chem.* **2009**, *48*, 10697.
(23) Alain, M.; Jacques, M.; Diane, M. B.; Karine, P. *J. Phys. Conf. Ser.* **2009**, *190*, 012034.
(24) Ankudinov, A. L.; Ravel, B.; Rehr, J. J.; Conradson, S. D. *Phys. Rev. B* **1998**, *58*, 7565.
(25) Skarstad, P. M.; Geller, S. *Mater. Res. Bull.* **1975**, *10*, 791.

(26) Stone, D.; Liu, J.; Singh, D. P.; Muratore, C.; Voevodin, A. A.; Mishra, S.; Rebholz, C.; Ge, Q.; Aouadi, S. M. *Scr.Mater.* **2010**, *62*, 735.
(27) Rietveld, H. M. *J. Appl. Crystallogr.* **1969**, *2*, 65.
(28) Gavriliu, S.; Lungu, M.; Lucaci, M.; Enescu, E. *J. Optoelectron. Adv. Mater.* **2006**, *8*, 702.
(29) van den Berg, A. J.; Juffermans, C. A. H. *J. Appl. Crystallogr.* **1982**, *15*, 114.
(30) Bish, D. L.; Post, J. E. *Am. Mineral.* **1993**, *78*, 932.
(31) http://www.ing.unitn.it/~maud/.
(32) Lutterotti, L.; Matthies, S.; Wenk, H. R.; Schultz, A. J.; Richardson, J. J. *J. Appl. Phys.* **1997**, *81*, 594.
(33) Will, G. *Powder diffraction: The Rietveld method and the two stage method to determine and refine crystal structures from powder diffraction data*;Springer-Verlag: Berlin, 2006;pp 44−69.
(34) Gracia, L.; Longo, V. M.; Cavalcante, L. S.; Beltrán, A.; Avansi, W.; Li, M. S.; Mastelaro, V. R.; Varela, J. A.; Longo, E.; Andrés, J. *J. Appl. Phys.* **2011**, *110*, 043501.
(35) Okumura, K.; Tomiyama, T.; Shirakawa, S.; Ishida, S.; Sanada, T.; Arao, M.; Niwa, M. *J. Mater. Chem.* **2011**, *21*, 229.
(36) Moscovici, J.; Rougier, A.; Laruelle, S.; Michalowicz, A. *J. Chem. Phys.* **2006**, *125*, 124505.
(37) Yamazoe, S.; Hitomi, Y.; Shishido, T.; Tanaka, T. *J. Phys. Chem. C* **2008**, *112*, 6869.
(38) Hasnain, S. S. *Report on the International Workshops on Standards and Criteria in XAFS. in X-ray Absorption Fine Structure: Proceedings of the VI International Conference on X-ray Absorption Fine Structures*; Ellis Horwood:New York, 1991.
(39) Momma, K.; Izumi, F. *J. Appl. Crystallogr.* **2011**, *44*, 1272.
(40) http://en.wikipedia.org/wiki/Octahedron.
(41) http://en.wikipedia.org/wiki/Deltahedron.
(42) http://en.wikipedia.org/wiki/Tetrahedron.
(43) http://en.wikipedia.org/wiki/Molecular_symmetry.
(44) Cavalcante, L. S.; Batista, F. M. C.; Almeida, M. A. P.; Rabelo, A. C.; Nogueira, I. C.; Batista, N. C.; Varela, J. A.; Santos, M. R. M. C.; Longo, E.; Li, M. S. *RSC Adv.* **2012**, *2*, 6438.
(45) Clark, G. M.; Doyle, W. P. *Spectrochim. Acta* **1966**, *22*, 1441.
(46) Siriwong, P.; Thongtem, T.; Phuruangrat, A.; Thongtem, S. *CrystEngComm* **2011**, *13*, 1564.
(47) Sczancoski, J. C.; Cavalcante, L. S.; Marana, N. L.; da Silva, R. O.; Tranquilin, R. L.; Joya, M. R.; Pizani, P. S.; Varela, J. A.; Sambrano, J. R.; Li, M. S.; Longo, E.; Andrés, J. *Curr. Appl. Phys.* **2010**, *10*, 614.
(48) Cavalcante, L. S.; Sczancoski, J. C.; Tranquilin, R. L.; Varela, J. A.; Longo, E.; Orlandi, M. O. *Particuology* **2009**, *7*, 353.
(49) Cheng, L.; Shao, Q.; Shao, M.; Wei, X.; Wu, Z. *J. Phys. Chem. C* **2009**, *113*, 1764.
(50) Marques, V. S.; Cavalcante, L. S.; Sczancoski, J. C.; Alcantara, A. F. P.; Orlandi, M. O.; Moraes, E.; Longo, E.; Varela, J. A.; Li, M. S.; Santos, M. R. M. C. *Cryst. Growth Des.* **2010**, *10*, 4752.
(51) Limpert, E.; Stahel, W.; Abbt, M. *BioScience* **2001**, *51*, 341.
(52) Kubelka, P.; Munk-Aussig, F. *Z. Tech. Physik* **1931**, *12*, 593.
(53) Myrick, M. L.; Simcock, M. N.; Baranowski, M.; Brooke, H.; Morgan, S. L.; Mccutcheon, J. N. *Appl. Spectrosc. Rev.* **2011**, *46*, 140.
(54) Smith, R. A. *Semiconductors*, 2nd ed.; Cambridge University Press: London, 1978; p 434.
(55) Kim, D. W.; Cho, I. S.; Lee, S.; Bae, S. T.; Shin, S. S.; Han, G. S.; Jung, H. S.; Hong, K. S. *J. Am. Ceram. Soc.* **2010**, *93*, 3867.
(56) Cavalcante, L. S.; Longo, V. M.; Sczancoski, J. C.; Almeida, M. A. P.; Batista, A. A.; Varela, J. A.; Orlandi, M. O.; Longo, E.; Li, M. S. *CrystEngComm* **2012**, *14*, 853.
(57) Anicete-Santos, M.; Picon, F. C.; Alves, C. N.; Pizani, P. S.; Varela, J. A.; Longo, E. *J. Phys. Chem. C* **2011**, *115*, 12180.
(58) Anicete-Santos, M.; Orhan, E.; de Maurera, M. A. M. A.; Simoes, L. G. P.; Souza, A. G.; Pizani, P. S.; Leite, E. R.; Varela, J. A.; Andrés, J.; Beltran, A.; Longo, E. *Phys. Rev. B* **2007**, *75*, 165105.
(59) Longo, V. M.; Cavalcante, L. S.; Paris, E. C.; Sczancoski, J. C.; Pizani, P. S.; Li, M. S.; Andrés, J.; Longo, E.; Varela, J. A. *J. Phys. Chem. C* **2011**, *115*, 5207.
(60) Tang, J.; Ye, J. *J. Mater. Chem.* **2005**, *15*, 4246.
(61) Tang, J.; Zou, Z.; Ye, J. *J. Phys. Chem. B* **2003**, *107*, 14265.
(62) Pereira, P. F. S.; de Moura, A. P.; Nogueira, I. C.; Lima, M. V. S.; Longo, E.; de Sousa Filho, P. C.; Serra, O. A.; Nassar, E. J.; Rosa, I. L. V. *J. Alloys Compd.* **2012**, *526*, 11.
(63) Almeida, M. A. P.; Cavalcante, L. S.; Li, M. S.; Varela, J. A.; Longo, E. *J. Inorg. Organomet. Polym.* **2012**, *22*, 264.